https://doi.org/10.22226/2410-3535-2022-4-354-359

Simulation of deformation and growth during surfacing of aluminum bronze nanograins

A. Yu. Nikonov[†,1,2], D. V. Lychagin[1,2], A. A. Bibko[1,2], O. S. Novitskaya[1]

[†]anickonoff@ispms.ru

[1]Institute of Strength Physics and Material Science of the RAS, Tomsk, 634055, Russia
[2]Tomsk State University, Tomsk, 634050, Russia

In additive manufacturing, it is important to determine the technological and structural factors that control the crystallization process and specify the required structure of the product. The crystallization structure is affected by the parameters of the starting material and the crystallization conditions. Using the orientation of the grains of the substrate, which is formed after electron-beam surfacing of aluminum bronze, the modeling parameters were set by the molecular dynamics simulation. The process of deformation of three adjacent grains under constrained conditions and structural changes in the process of interaction with a melt drop and subsequent crystallization were considered. An analysis of grain deformation made it possible to reveal the role of geometric shear stress concentrators and to determine the significance of constrained conditions for deformation of polycrystal grains. It has been established that under the influence of a drop of melt, stacking faults are the least thermally stable, and twins are the most stable. The crystallographic orientation of the crystallizing grains coincides with the orientation of the substrate grains. During crystallization, columnar grains continue to grow, in which stacking faults and twins are formed.

Keywords: aluminum bronze, molecular dynamics simulation, electron beam surfacing, deformation, crystallization, grains.

1. Introduction

Recently, significant progress has been made in understanding the physical processes of the metals and alloys additive manufacturing. This makes it possible to obtain products with a given structure and predictable properties. A comprehensive review of the main 3D printing methods, materials, and the forecast for the development of additive manufacturing is given in reviews [1–5]. The scope of laser melting [6–12] and electron beam melting (EBM) [13–25] for the production of metal products is expanding. Using electron beam melting, products are obtained from steels [13,14], high entropy alloys [15,16], nickel-base superalloys [17,18], titanium [19], Ti-alloy [20,21], and other metals and alloys. This method is used to obtain products from copper-based alloys, in particular, aluminum bronze [22–25].

In products during 3D surfacing, one of the main structural parameters is the orientation and morphology of grains growing during melt crystallization. As a result, "texture by design" [4] and "structural design" are formed, which determine the functional properties of the product along with design features. In this regard, the main task of additive manufacturing is the adaptation of the alloy to the technology of additive manufacturing. The crystallization structure is largely determined by the temperature field and growth crystallography. The initial growth orientation is set by the grain orientation of the previous crystallized layer and is related to neighboring growing grains. Features of growth processes in small volumes can be studied using molecular dynamics simulation [26–32]. The method makes it possible to trace the crystallization processes, the consistency of crystal growth, and the thermodynamic stability of the structure in a nanovolume. The results obtained can be generalized to a larger volume while maintaining the principle of similarity due to the identity of the crystal structure of the material. The feasibility of the principle of similarity was shown when modeling deformation processes on fcc single- and polycrystals in comparison with the analysis of experimentally observed deformation, in particular, in polycrystals of aluminum bronze obtained by electron beam surfacing [33–35]. The objective of this study by the method of molecular dynamics is to establish the influence of the orientation of a group of grains and the boundaries between them on the deformation and subsequent crystallization during interaction with a melt drop in order to establish the patterns of formation of deformation defects, their thermal stability and the crystallization process.

2. Material and computational procedure

The object of research is the Cu-13 at.%Al alloy. Simulation was performed by the molecular dynamics method using the LAMMPS software package [36]. The interatomic interaction of the selected materials was described by the interatomic potential constructed within the embedded atom method (EAM) [37]. Interatomic potentials of the second nearest neighbor modified embedded-atom method (2NN-MEAM) are developed for binary aluminum (Al) alloys applicable from room temperature to the melting point [38].

The equations of atomic motion were integrated using the Verlet velocity method. The OVITO software [39] was used

to visualize and analyze the defective structure. The internal structure was studied using the common neighbor analysis (CNA) method [40] and the dislocation extraction algorithm (DXA) [41].

A Cu-13 at.%Al polycrystalline consisting of three grains was simulated. The geometry and crystallographic orientation were set based on the crystallographic analysis of the sample obtained by electron beam surfacing. The orientation map relative to the Y-axis, obtained by reflected electron diffraction, is shown in Fig. 1a. For the model, fragment A was selected, marked with a rectangle in Fig. 1a. A schematic representation of a model sample with dimensions of $100a \times 60a \times 30a$ (a is the lattice parameter) is shown in Fig. 1b. The lattice parameter was calculated by relaxing an infinitely extended bronze single crystal at zero pressure and a given temperature. The number of atoms in the sample is about 710 000. The following orientations of the crystal lattice along the X, Y, and Z axes were set: grain 1 — $[\bar{7}\,2\bar{1}\,\bar{6}0]$, $[3\bar{1}0]$ and $[\bar{6}\,\bar{1}8\,7]$; grain 2 — $[\bar{1}\,\bar{2}\,3]$, $[5\bar{4}\,1]$and $[\bar{1}\,\bar{1}\,1]$; grain 3 — $[1\,2\,\bar{2}]$, $[4\,\bar{1}\,1]$ and $[0\,\bar{1}\,\bar{1}]$. The difference in directions between the experimental data and the model is due to the error in determining the directions. For the model, the values closest to the experiment were taken that satisfy the orthogonally condition. It was assumed that the grain boundaries were located perpendicular to the image plane.

The uniaxial deformation of the sample was set by moving atomic layers with dimensions of $130a \times 3a \times 60a$ at a constant speed of 2.5 m/s, calculating X0Z above and below the sample in the frame (orientation of the direction of observation along the Y-axis). The results were made up of three grains, which continued the grains of the loaded sample. In addition, constrained deformation conditions were set in the sides of three lateral faces of the *xzx* type (shear limitation along the X-axis and in the –Z direction). To do this, a virtual fixed plane was located along the surface of the lateral face. Sample atoms that crossed this plane were subjected to additional forces calculated by the formula $F(r) = -Kr^2$. Here K is the coefficient and r is the shortest distance from the plane to the atom. These conditions imitate the deformation of the surface grains of a polycrystal. Sample atoms were considered as an NVT ensemble at a temperature of 300 K.

To simulate structural changes during surfacing of a deformed group of grains on the surface (the process was discussed above), a drop (consisting of 540 000 atoms) heated to a temperature of 1500 K was lowered. An additional force directed towards the substrate was set to move the drop. After contact of the drop with the substrate, the sample was cooled to 300 K for 3.3 ns.

3. Results and discussion

3.1. Simulation of plastic deformation of a group of grains with given orientation

A group of three grains with given crystallographic parameters was subjected to compressive deformation in a model experiment. The sequence of dislocation slip with the formation of stacking faults is shown in Fig. 2.

Deformation begins in grain 3, which has a compression axis. The sliding starts along plane 1 and then along plane 2 (Fig. 2 a). Practically simultaneously with the shear along plane 2, sliding begins in central grain 2 (planes 3 and 4), and then in grain 1 (plane 5). A characteristic moment of deformation is the formation of an intrinsic stacking defect during sliding, which can then be destroyed during repeated sliding in this plane. The onset of shear, as a rule, develops from geometric stress concentrators, which are the edges of the sample and the corner joints of the grains. Generation of shears from one grain to another grain is not observed. Shear planes (intrinsic stacking faults in the figure) in one grain are not spatially related to planes in an adjacent grain. With 4% deformation in the central grain 2, deformation twins begin to form. A system of deformation twins (I in Fig. 2 e) is formed in the angular deformation domains. The main system of twins is formed in the main volume (II in Fig. 2 e). In other grains, in the strain range under study, twins are not formed, and intrinsic and extrinsic stacking faults are observed.

The slip of dislocations inside the grains is accompanied by the formation of a deformation relief on the surface. To compare the results of the experiment and simulation, Fig. 3 shows an orientation map with a superimposed pattern of the deformation relief and a relief on the surfaces of the simulated grains.

From the set of active slip systems observed in the simulation (Fig. 1a), systems with the maximum Schmid factor (shown in Fig. 3 a), which are typical for the central regions of grains, were realized in the experiment. In general, there is a good agreement between the experimentally observed results and the results obtained by simulating the deformation process by the molecular dynamics method.

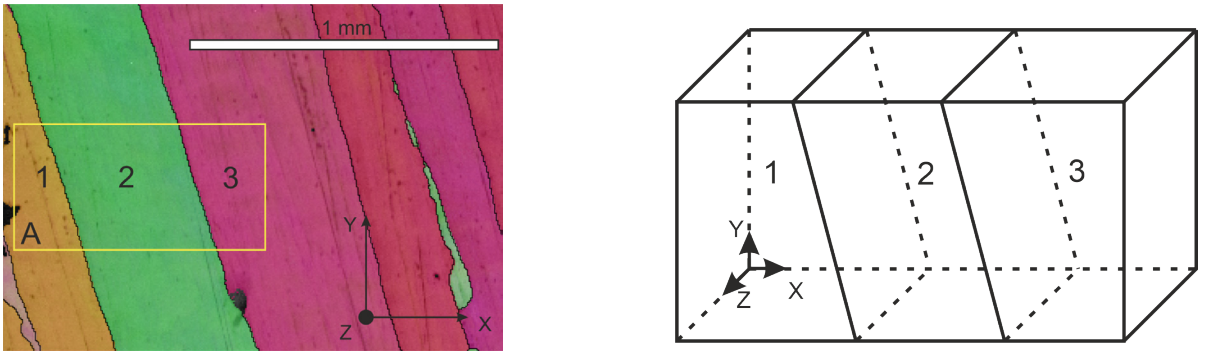

a b

Fig. 1. (Color online) Grain map obtained by electron backscatter diffraction (a) and the schematic structure of the model built on its basis (b).

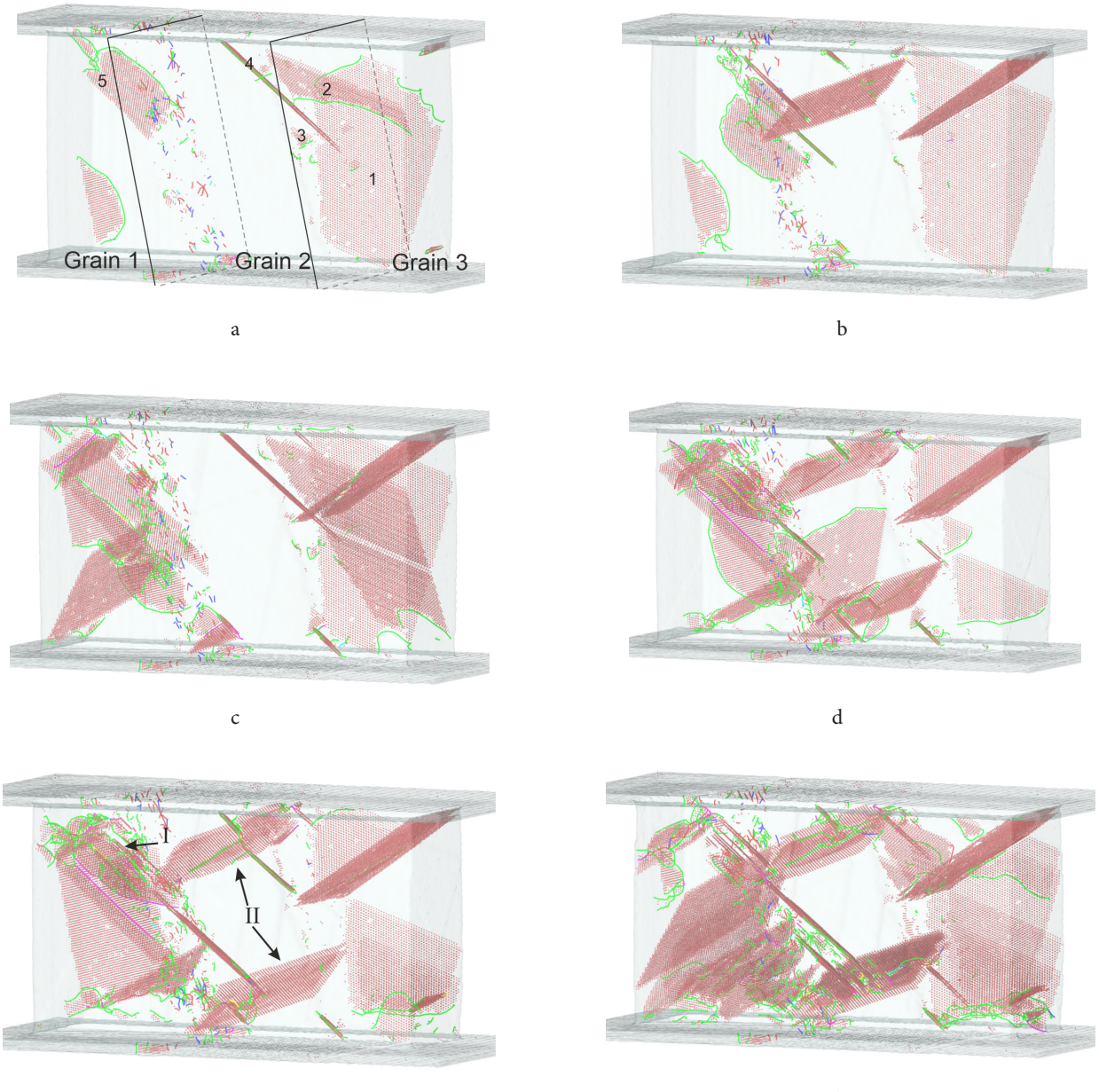

a b c d e f

Fig. 2. (Color online) Evolution of the shear pattern in a system of three grains: ε = 0.65% (a); ε = 1.12% (b); ε = 2.98% (c); ε = 4.38% (d); ε = 5.32% (e); ε = 7.64% (f).

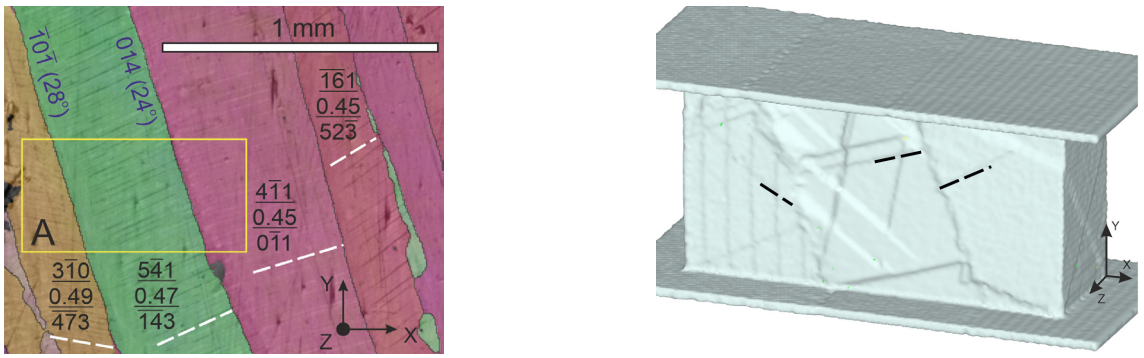

a b

Fig. 3. (Color online) Slip lines in grains of aluminum bronze deformed by 7%, obtained by electron beam surfacing (a), and deformation relief of the simulated area A (b). Designations in (a): fraction in the grain is the orientation of the load axis Y; the Schmid factor of the shear system, which forms the slip line; the normal to the grain plane Z and the inscription along the grain boundary are the crystallographic direction of the misorientation axis and the misorientation angle.

The main features of the accumulation of defects correspond to the processes that are observed during the deformation of single crystals [35]. The closest orientation of the deformation axis is at the corners of the inverse stereographic triangle for the outer grains <100>, while the lateral faces have the same indices. For the right grain, the closest "ideal" orientation of the lateral faces is {110}, and for the leftmost grain, their orientation is closer to {001}. The closest orientation to the corners of the inverse stereographic triangle of the deformation axis of the middle grain is <011>, and of the cases considered in the simulation, the variant with the combination of lateral faces {111} and {112} is the closest. When considering the case of shear limitation from three lateral faces, the free face of the first grain is the face approaching {001}, the second — {112} and the third — {011}. It should be noted here that, according to the results of previous simulations on single crystals, shear limitation promotes twinning and faster accumulation of dislocations in the bulk of the single crystal. This is especially important for the orientation of the deformation axis close to <011>. In the absence of shear limitation to the sides of the lateral faces, partial dislocations practically do not remain in the body of the single crystal, leaving on the lateral faces. As in the case of the deformation of fcc single crystals [33 – 35], when modeling the deformation of a group of grains, the leading role of geometric stress concentrators (edges near end) on the localization of shear initiation sites is retained. The grain boundaries of the considered geometry do not play a significant role in shear initiation. There is no generation of shear through the grain boundary into the neighboring grain. Linking the geometric arrangement of stress concentrators in grains of different morphology, the results of the study by Yuana L. et al [42] become clear: the dislocation density and the formation of sessile dislocations in case the layer-grained models more.

3.2. Simulation of the interaction of a substrate with a melt drop

The structure of the deformed sample before surfacing is shown in Fig. 4 a, b. Each deformed grain contains stacking faults and twins. When the heated drop is lowered onto the sample, it is heated and partially refined. As a result, stacking faults closest to the surface are destroyed (Fig. 4 c, d). With further exposure, some of the twins disappear (Fig. 4 e, f). These results show that the thermal stability of twins is higher than that of stacking faults. Here, one can also note the beginning of droplet crystallization (an increase in the area occupied by the atoms of the base material (green area in Fig. 4 g).

Stacking faults and twins are formed in the region of crystallization (Fig. 4 h). During crystallization, the growth of each grain continues, maintaining the previous orientation of each crystallite. Elongated grains are formed in the direction of the deposited surface. This confirms the experimentally observed regularity of the formation of macroscopic columnar grains during surfacing [24]. The resulting systems of defects in the crystallizing regions inherit the orientation of the defects in their parental part.

This result of thermal stability and crystallization is characteristic only for the selected simulation parameters.

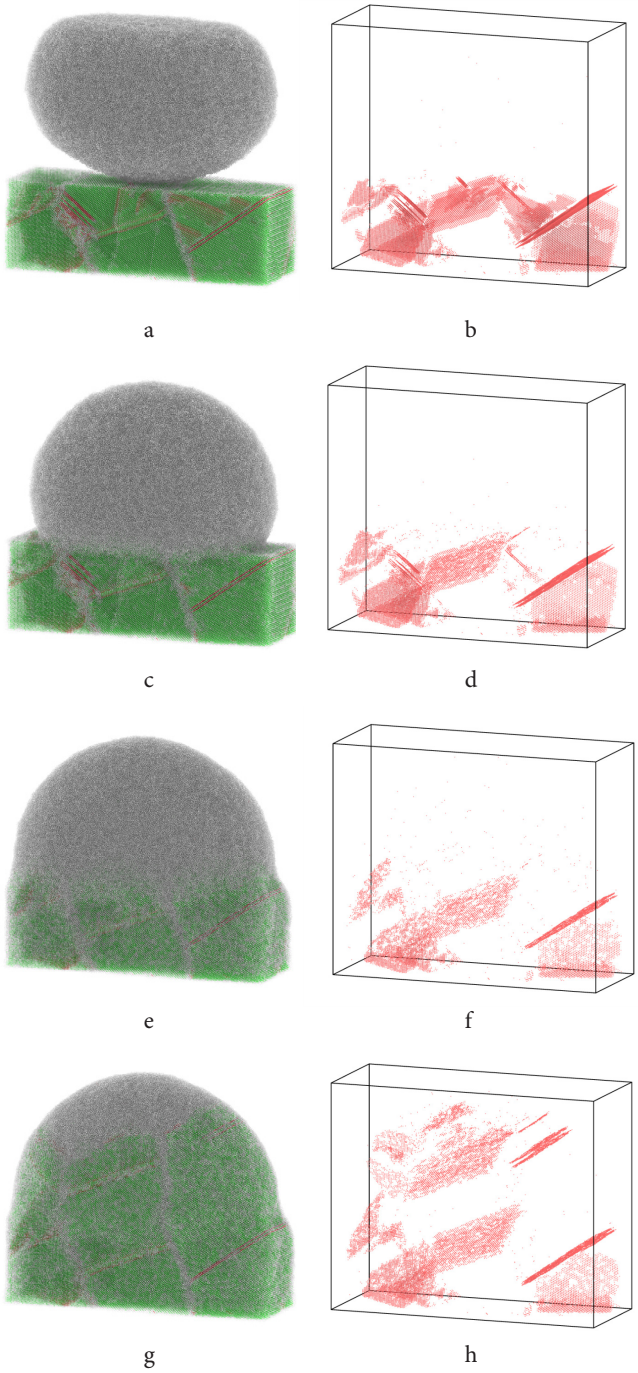

Fig. 4. (Color online) Structural changes during the interaction of a melt drop with a polycrystalline sample (b, d, f, h are the bulk of the sample): 0.15 ns (a, b); 0.35 ns (c, d); 1.50 ns (e, f); 3.25 ns (g, h).

The cooling rate variation shows the presence of a critical rate for stable dislocation defects and grain boundaries emerge [27]. The size, grain morphology, and growth crystallographic direction determine the performances of metallic product. During surfacing, layers with grains of different morphology are formed [24]: columnar grains and non-columnar or "spherical" grains. As the results of experiment [24, 35, 43] and modeling [43 – 45] show, the columnar grains and near-cubic texture are dominant in the solidification process. It's connected with competitive grain growth and the heat flow characteristics. It has been shown that the location of the heat sink surface [9, 25, 43] and the direction of surfacing [46] affect the feature of the crystallization structure in a

macro volume. Thus, when analyzing the regularities of grain growth, this work takes into account only the local case of grain growth during crystallization, which is determined by the crystallography of grains of the substrate and the thermal parameters of the melt drop.

4. Conclusions

Previous molecular dynamics simulation of deformation by compression of fcc metals and Cu-Al alloy single- and polycrystals [33 – 35] showed good agreement with the experimentally observed picture of the deformation relief. The development of the EBSD made it possible to obtain the crystallographic characteristics of the grains of the material surfaced using 3D technology. The obtained crystallographic characteristics of the area containing three grains were set as modeling parameters during deformation and then interaction with a melt drop. The analysis of the experimentally observed and simulated shear pattern [35] is supplemented by the results of consideration of the development of defects formed during deformation. The role of geometric stress concentrators, previously established for fcc single crystals, is confirmed for a system of three grains. Shear limitation towards the side faces of the grains reduces the possibility of dislocations reaching the surface and thereby increase the dislocation density inside the grain. The grain boundaries of a given structure do not affect the shear initiation. At the considered degrees of deformation, shear generation through the grain boundary does not occur.

The analysis of structural changes during the interaction of a melt drop with a substrate showed that stacking faults are the least thermally stable. For their destruction, not only sufficient temperature is required, but also sufficient time. During crystallization, the crystallographic orientation of the substrate grains is inherited. As the crystals grow, stacking faults and twins form in them.

Acknowledgements. This research was funded the Research Program 20-72-10184 of the Russian Science Foundation for 2020 – 2023.

References

1. T. D. Ngo, A. Kashani, G. Imbalzano, K. T. Q. Nguyen, D. Hui. Compos. Part B Eng. 143, 172 (2018). Crossref
2. T. DebRoy, H. L. Wei, J. S. Zuback, T. Mukherjee, J. W. Elmer, J. O. Milewski, A. M. Beese, A. Wilson-Heid, A. De, W. Zhang. Prog. Mater. Sci. 92, 112 (2018). Crossref
3. B. Blakey-Milner, P. Gradl, G. Snedden, M. Brooks, J. Pitot, E. Lopez, M. Leary, F. Berto. Mater. Des. 209, 110008 (2021). Crossref
4. A. T. Clare, R. S. Mishra, M. Merklein, H. Tan, I. Todd, L. Chechik, J. Li, M. Bambach. J. Mater. Process. Technol. 299, 117358 (2022). Crossref
5. M. A. Mahmood, D. Chioibasu, A. Ur Rehman, S. Mihai, A. C. Popescu. Metals. 12, 77 (2022). Crossref
6. G. P. Dinda, A. K. Dasgupta, J. Mazumder. Surf. Coatings Technol. 206 (8 – 9), 2152 (2012). Crossref
7. G. P. Dinda, A. K. Dasgupta, J. Mazumder. Scr. Mater. 67 (5), 503 (2012). Crossref
8. L. Thijs, F. Verhaeghe, T. Craeghs, J. Van Humbeeck, J.-P. Kruth. Acta Mater. 58 (9), 3303 (2010). Crossref
9. A. Piglione, B. Dovgyy, C. Liu, C. M. Gourlay, P. A. Hooper, M. S. Pham. Mater. Lett. 224, 22 (2018). Crossref
10. M. Garibaldi, I. Ashcroft, M. Simonelli, R. Hague. Acta Mater. 110, 207 (2016). Crossref
11. M. Muhammad, P. D. Nezhadfar, S. Thompson, A. Saharan, N. Phan, N. Shamsaei. Int. J. Fatigue. 146, 106165 (2021). Crossref
12. N. T. Aboulkhair, M. Simonelli, L. Parry, I. Ashcroft, C. Tuck, R. Hague. Prog. Mater. Sci. 106, 100578 (2019). Crossref
13. Y. Zhong, L.-E. Rännar, L. Liu, A. Koptyug, S. Wikman, J. Olsen, D. Cui, Z. Shen. J. Nucl. Mater. 486, 234 (2017). Crossref
14. I. A. Segura, J. Mireles, D. Bermudez, C. A. Terrazas, L. E. Murr, K. Li, V. S. Y. Injeti, R. D. K. Misra, R. B. Wicker. J. Nucl. Mater. 507, 164 (2018). Crossref
15. R. S. Mishra, R. S. Haridas, P. Agrawal. Mater. Sci. Eng. A. 812, 141085 (2021). Crossref
16. S. M. Gaytan, L. E. Murr, E. Martinez, J. L. Martinez, B. I. Machado, D. A. Ramirez, F. Medina, S. Collins, R. B. Wicker. Metall Mater Trans A. 41, 3216 (2010). Crossref
17. M. Ramsperger, R. F. Singer, C. Körner. Metall. Mater. Trans. A. 47 (3), 1469 (2016). Crossref
18. C. Körner, M. Ramsperger, C. Meid, D. Bürger, P. Wollgramm, M. Bartsch, G. Eggeler. Metall. Mater. Trans. A. 49 (9), 3781 (2018). Crossref
19. P. Heinl, A. Rottmair, C. Körner, R. F. Singer. Adv. Eng. Mater. 9 (5), 360 (2007). Crossref
20. S. Liu, Y. C. Shin. Mater. Des. 164, 107552 (2019). Crossref
21. D. A. Ramirez, L. E. Murr, E. Martinez, D. H. Hernandez, J. L. Martinez, B. I. Machado, F. Medina, P. Frigola, R. B. Wicker. Acta Mater. 59 (10), 4088 (2011). Crossref
22. W. Lu, W. Zhai, J. Wang, X. Liu, L. Zhou, A. M. M. Ibrahim, X. Li, D. Lin, Y. M. Wang. Addit. Manuf. 38, 101751 (2021). Crossref
23. W. Zhai, Y. Zhao, R. Zhou, W. Lu, W. Zhai, X. Liu, L. Zhou, S. Chang. Mater. Charact. 184, 111706 (2022). Crossref
24. E. S. Khoroshko, A. V. Filippov, S. Yu. Tarasov, N. N. Shamarin, E. N. Moskvichev, S. V. Fortuna, D. V. Lychagin, E. A. Kolubaev. Metals. 10, 1568 (2020). Crossref
25. V. Romanova, O. Zinovieva, R. Balokhonov, E. Dymnich, E. Moskvichev, A. Filippov, D. Lychagin. Addit. Manuf. 48, 102415 (2021). Crossref
26. N. Zhou, X. Wei, L. Zhou. Crystals. 8, 346 (2018). Crossref
27. G. Singh, A. M. Waas, V. Sundararaghavan. Comput. Mater. Sci. 200, 110807 (2021). Crossref
28. R. Ma, L. Zhou, Y. Liang, Q. Chen, Z. Tian, R. Liu, Y. Mo, T. Gao, Q. Xie. Curr. Appl. Phys. 29, 18 (2021). Crossref
29. R. Namakian, B. R. Novak, X. Zhang, W. J. Meng, D. Moldovan. Appl. Surf. Sci. 570, 151013 (2021). Crossref
30. A. Brant, M. Sundaram. Precis. Eng. 56, 412 (2019). Crossref
31. Y. Tang, C. Xie, J. Chen, X. Wang. Metals (Basel). 12 (4), 633 (2022). Crossref
32. Z. Cui, X. Zhou, Q. Meng. Metals (Basel). 10 (12), 1660 (2020). Crossref

33. D. Lychagin, A. Dmitriev, A. Nikonov, E. Alfyorova. Crystals. 10 (8), 666 (2020). Crossref
34. A.Y. Nikonov, A.I. Dmitriev, D.V. Lychagin, L.L. Lychagina, A.A. Bibko, O.S. Novitskaya. Metals (Basel). 11 (4), 582 (2021). Crossref
35. A.Y. Nikonov, D.V. Lychagin, A.A. Bibko, O.S. Novitskaya. Metals (Basel). 12 (1), 114 (2022). Crossref
36. S. Plimpton. J. Comput. Phys. 117 (1), 1 (1995). Crossref
37. J. Cai, Y.Y. Ye. Phys. Rev. B. 54 (12), 8398 (1996). Crossref
38. A. Mahata, T. Mukhopadhyay, M.A. Zaeem. Comput. Mater. Sci. 201, 110902 (2022). Crossref
39. A. Stukowski. Model. Simul. Mater. Sci. Eng. 18 (1), 015012 (2010). Crossref
40. J.D. Honeycutt, H.C. Andersen. J. Phys. Chem. 91 (19), 4950 (1987). Crossref
41. A. Stukowski, V.V. Bulatov, A. Arsenlis. Model. Simul. Mater. Sci. Eng. 20 (8), 085007 (2012). Crossref
42. L. Yuan, P. Jing, R. Shivpuri, C. Xu, Z. Xu, D. Shan, B. Guo. Philos. Mag. 99 (22), 2818 (2019). Crossref
43. Y. Zhao, Y. Koizumi, K. Aoyagi, D. Wei, K. Yamanaka, A. Chiba. Materialia. 6, 100346 (2019). Crossref
44. D. Zöllner. Comput. Mater. Sci. 200, 110803 (2021). Crossref
45. C. Guo, K. Weng, J. Wang, H. Zhao, X. Dong, Y. Fan, J. Li. Comput. Mater. Sci. 210, 111061 (2022). Crossref
46. L. Sun, X. Ren, J. He, Z. Zhang. J. Mater. Sci. Technol. 67, 11 (2021). Crossref